Vadim V. Silberschmidt
Editor

International Centre for Mechanical Sciences

Computational and Experimental Mechanics of Advanced Materials

CISM Courses and Lectures, vol. 514

SpringerWienNewYork

SpringerWienNewYork

CISM COURSES AND LECTURES

The series presents lecture notes, monographs, edited works and proceedings in the field of Mechanics, Engineering, Computer Science and Applied Mathematics.
Purpose of the series is to make known in the international scientific and technical community results obtained in some of the activities organized by CISM, the International Centre for Mechanical Sciences.

INTERNATIONAL CENTRE FOR MECHANICAL SCIENCES

COURSES AND LECTURES - No. 514

COMPUTATIONAL AND EXPERIMENTAL MECHANICS OF ADVANCED MATERIALS

EDITED BY

VADIM V. SILBERSCHMIDT
LOUGHBOROUGH UNIVERSITY, LOUGHBOROUGH, LEICESTERSHIRE,
GREAT BRITAIN

SpringerWienNewYork

This volume contains 106 illustrations

Printed in Italy
SPIN 12753598

All contributions have been typeset by the authors.

ISBN 978-3-211-99684-3 SpringerWienNewYork

PREFACE

Advanced materials (composites, multiphase materials, materials for microelectronics, biomaterials, etc.) play a crucial role in modern engineering and biomechanical applications where they are often exposed to complex loading and environmental conditions. In many cases, new approaches are needed to characterise various features of these materials and to model their deformational behaviour, failure processes as well as to analyse reliability of components and structures under different conditions. Such approaches should be calibrated and validated by specific experimental techniques, quantifying both microstructural features and respective mechanisms at various length scales. The aim of the course is to give an overview of various modelling tools and experimental methods that can be employed to analyse and estimate properties and performance of advanced materials.

The first paper (by P.D. Ruiz and V.V. Silberschmidt) deals with experimental analysis of mechanical behaviours of advanced materials. A special emphasis is on techniques used to gain quantitative microstructural information needed for material modelling and/or experimental validation of model predictions. Two main groups of techniques are covered - mechanical tests and full-field analysis. The paper starts with application of dynamic mechanical analysis to viscoelastic materials followed by a discussion of experimentation with microspecimens. Theoretical aspects of nanoindentation are presented together with case studies for a Ni-based alloy and ceramic coating. A review of full-field measuring techniques is accompanied by examples of their use to validate predictions of stresses in adhesive joints and surface strains, damage detection and characterisation as well as identification of material's parameters.

Another part of the course deals with modern theoretical approaches used to analyse heterogeneous materials and a non-linear material behaviour. The first topic is covered in a paper by G.S. Mishuris, A.B. Movchan and L.I. Slepyan that reviews main results obtained for periodic structures based on dynamic lattice Green's functions. Among the analysed phenomena are localization of vibrations near defects and fracture in structured media, including wave tunnelling along the crack and energy dissipation in the lattice containing a moving crack. In the next paper (by M. Jabareen and M.B. Rubin) the second topic

is studied by means of the formulation of a 3-D brick Cosserat Point Element (CPE) for the solution of problems in non-linear elasticity. The paper opens with a review of some tensor operations and kinematic measures in continuum mechanics followed by introduction of the CPE that exhibits no locking for nearly incompressible materials and for thin structures, like plates and shells. Some example problems for such structures are discussed.

A paper by E. Busso reviews multiscale materials modelling approaches required to complement continuum and atomistic analyses methods. Their potential for computational materials design, based on the understanding of the dual nature of the structure of matter - continuous when viewed at large length scales and discrete when viewed at an atomic scale - is discussed. Various methods of continuum mechanics are reviewed, including a local crystallographic framework and non-local approaches. The paper finishes with a discussion of the problem of bridging the length and time scales. Another paper (by H.J. Böhm, D.H. Pahr and T. Daxner) deals with numerically based continuum modelling of thermomechanical and thermophysical behaviours of microstructured materials. After a review of mean-field methods and variational bounds the authors discuss various aspects of, and methods for, modelling discrete microstructures. Among the presented applications are elastoplastic composites at finite strains, diamond particle-reinforced composites as well as porous and cellular materials.

In the final paper by V.V. Silberschmidt, several case studies are analysed in order to demonstrate the strategies used to solve the real-life problems, in which the microstructure of materials directly affects their response to loading and/or environmental conditions. Among the presented examples are studies of the effect of microstructural randomness of carbon fibre-reinforced composites and ceramic coatings on their properties and performance as well as incorporation of microstructure and various deformational mechanisms in models of flip chip microelectronic packages.

The book is addressed to doctoral students, young researchers as well as practicing R&D engineers, dealing with advanced materials, components and structures.

Vadim V. Silberschmidt

CONTENTS

Experimental Analysis of Mechanical Behaviour of Advanced Materials

Pablo D. Ruiz and Vadim V. Silberschmidt

Wolfson School of Mechanical and Manufacturing Engineering,
Loughborough University, UK

1 Introduction

A notion of a material's mechanical property in many cases is not an unambiguous one. There are two main groups of reasons for this. The first is linked to *conditions* of the test, the second to the *length scale*, for which property is sought. Hence, instead of a narrow understanding of a mechanical property as a constant magnitude obtained from the handbook or a database, modern researchers dealing with real-life applications of advanced materials should rather consider it as a multi-parametric function and, in some cases, even a statistic one.

Let us start with analysis of the first group since it has direct implications for performing the tests to obtain material's properties. The effect of *environmental* conditions on mechanical parameters of materials is mostly appreciated in terms of temperature-dependent properties. Other environmental factors could be also important for some specific applications (e.g. hygroscopic effect in composites, exposure to aggressive environment, irradiation effects etc.) but they are outside the scope of this Chapter. Another important factor is the *loading rate*, affecting non-elastic response of various materials, e.g. strain-rate hardening in plasticity and strain-rate sensitivity of a viscous behaviour. A *type of loading* is also important, especially for strength assessment – consider the differences between the (quasi)static strength, on the one hand, and dynamic (impact) and cyclic loading (fatigue) strengths, on the other. A *loading state*, used in experiments, is usually supposed to be simple and permanent (i.e. non-changing during the experiment); an implementation of these requirements can become rather cumbersome in cases of large deformations.

An importance of the *length scale* is linked to microscopic heterogeneity of most materials. This can be complicated by a presence of several levels of non-

uniformity, e.g. in layered structures with different properties of layers, functionally-graded materials etc. Hence, two levels of properties assessment are possible. For specimens larger than the size of *representative volume element* (*RVE*), or, in other words, containing a large representative set of microstructural features (grains, microdefects, reinforcing elements in composites etc.) – *effective* (sometimes called *global* or *homogenized*) properties are obtained in tests. These magnitudes are usually presented in handbooks, databases etc. of material's properties. In contrast, properties measured at the lower length scale – known as *local properties* – demonstrate a considerable spatial scatter. The extent of the latter depends on the scale size (*window size*) – the smaller the window, the larger the scatter, which, in the case of two-phase materials will have two natural bounds linked to the properties of the constituents (Silberschmidt, 2008).

In many practical cases, the global properties cannot be used in models due to a large size of the RVE compared to characteristic dimensions of a component. Besides, a transition to critical and post-critical behaviour of materials that is characterised by the onset of plastic flow, macroscopic damage and/or failure is usually linked to *localisation* of these mechanisms precluding the use of effective parameters. One of the obvious examples is a transition from a macroscopically uniform deformation of a large specimen of polycrystalline material in the elastic regime to a spatially localised plastic flow, e.g. due shear band formation starting in grains that are appropriately oriented with respect to maximum shear stresses.

All the discussed features should be adequately accounted for in preparation of test programs and employment of specific techniques. This Chapter can by no means present a fully comprehensive description of all experimental techniques used to assess mechanical behaviour of materials. It rather deals with some specific types of tests that are usually not covered by standard textbooks on experimental mechanics dealing mainly with global properties. Since descriptions of the latter are (to some extent) ubiquitous, the authors decided to narrow down the choice of the techniques to those that either characterise more advanced properties (e.g. relaxation ones), local (microstructure-induced) properties or their spatial distribution – so called *full-field* methods.

2 DMA & visco-elastic properties

In contrast to elastic and plastic behaviour, characterisation of the visco-elastic one is still not a fully established in the engineering community. This can be explained by historic reasons linked to a relatively late broad introduction of plastics, demonstrating such behaviour, into various products, as compared to

traditional structural materials. High-temperature applications with a long-term exposure of components (made predominantly, of metals and alloys) to extreme thermal conditions became ubiquitous nearly at the same time. Another reason is unsuitability of standard tensile tests to provide a direct information about parameters characterising viscous behaviour in the same (relatively) simple way as for the elastic behaviour (Young's modulus) or the plastic one (yield stress, hardening modulus). Special tests – creep (loading with a constant stress level) and relaxation (loading with a constant deformation) – that can be nowadays performed with the same universal testing machines used for tensile testing are rather time-consuming when a full description of visco-elasticity is necessary.

Various applications can not be reduced to the cases of pure creep or relaxation; among the obvious examples are solder points/balls in microelectronic packages exposed to creep-fatigue under service conditions or plastics and composites under dynamic (e.g. impact) loading. The need for the parameters characterising the visco-elastic behaviour is additionally enhanced by expansion of mechanics of materials into domain of biomaterials, many of which can be considered as visco-elastic media.

A special type of tests – *dynamic mechanical analysis* (DMA) – was developed to characterise visco-elastic properties of materials. Let us start with some general ideas of visco-elasticity that will be analysed following classical books (Christensen, 1971 and Tschoegl, 1989).

The visco-elastic behaviour is often described in terms of a so-called *hereditary* approach with stress being dependent on the current strain state as well as the history of strain in the material. For a uniaxial loading at $t = 0$ of an isotropic linear visco-elastic material under isothermal conditions the constitutive equation can be introduced in terms of a hereditary integral (also known as *Boltzmann superposition* integral):

$$\sigma(t) = \int_{0_-}^{t} E(t-\tau)\dot{\varepsilon}(\tau)d\tau \,, \tag{1}$$

where $E(t)$ is a relaxation function, $\dot{\varepsilon}$ is a strain rate. Another form can be used to explicitly introduce the strain history:

$$\sigma(t) = E_e\left(\varepsilon(t) - \int_{0_-}^{t} \hat{E}(t-\tau)\dot{\varepsilon}(\tau)d\tau\right), \tag{2}$$

where E_e is an equilibrium modulus.

For the so called *generalised Maxwell model* (also known as *Wiechert model*) consisting of a spring and N Maxwell elements (see Figure 1) the relaxation

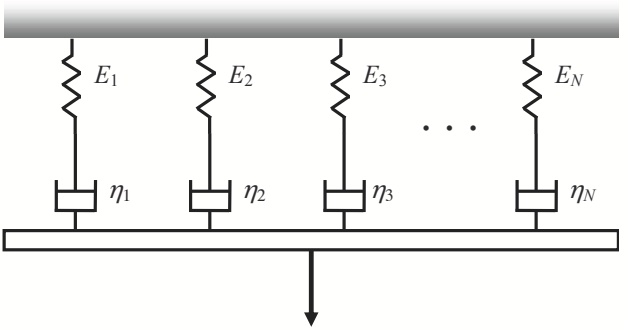

Figure 1. Generalised Maxwell model.

model has the following form:

$$E(t) = E_e + \sum_{i=1}^{N} E_i e^{-\frac{t}{t_{ti}}}, \tag{3}$$

where $t_i = \eta_i / E_i$ are relaxation times of elements. The second term is also known as the *Prony series*.

Using the Laplace transformation

$$\bar{f}(s) = \int_0^\infty f(t) e^{-st} dt, \tag{4}$$

an *operational modulus* (Park and Schapery, 1999) can be obtained in the following form:

$$\overline{E}(s) = s \int_0^\infty E(t) e^{-st} dt. \tag{5}$$

The frequency-dependent version of the stress relaxation modulus can be obtained for a steady-state harmonic (sinusoidal) loading with a frequency of oscillation ω:

$$E^*(\omega) = \overline{E}(s)\Big|_{s \to i\omega} = E'(\omega) + iE''(\omega), \tag{6}$$

where E' and E'' are the so called storage and loss moduli.

A more clear analysis can be obtained by comparison of the responses of different types of media to the harmonic excitation presented in Figure 2. Obviously, in a perfectly elastic media (Figure 2a) phases of strain and stress diagrams would coincide, since both strain and stress are directly proportional due to the Hooke's law. A perfectly viscous material is characterised by the known relationship between the stress and the strain rate: $\sigma = \eta\dot{\varepsilon}$ that means that in a system with harmonic strain excitation the stress level will change with a delay by $\varphi = \pi/2$ (Figure 2b).

A linear visco-elastic material is an intermediate case: for a harmonic excitation with strain the stress changes will be characterised by the phase difference δ (Figure 2c) that due to standard dynamic analysis (Inman, 2007)

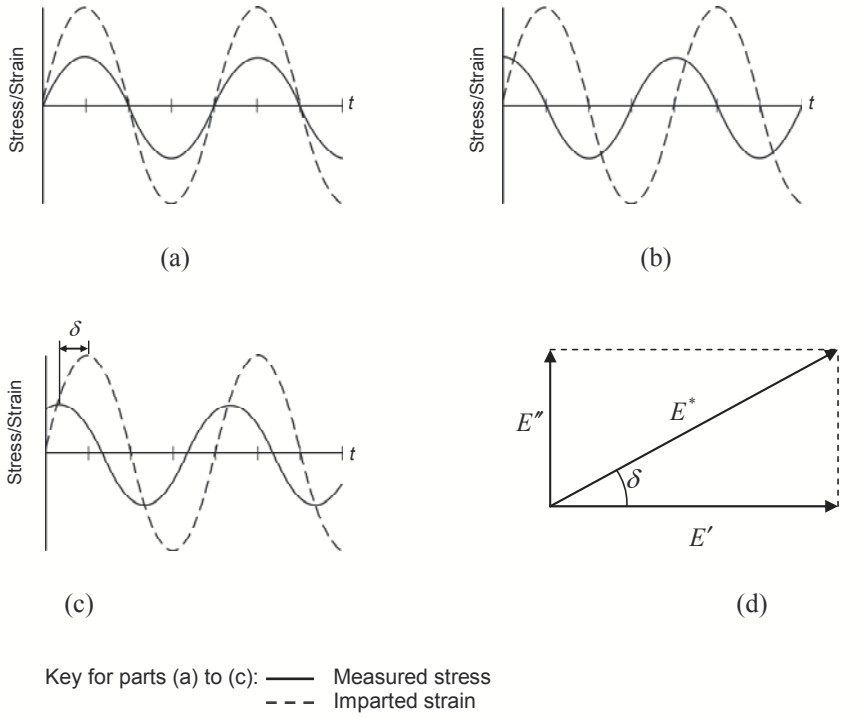

Figure 2. Cyclic stress strain diagrams for (a) elastic, (b) viscous and (c) visco-elastic materials, (d) complex modulus diagram for visco-elastic material.

can be determined as

$$\delta = \tan^{-1} \frac{E''}{E'}, \tag{7}$$

(see the respective *Argand diagram* in Figure 2d). The phase difference δ indicates the extent of material's viscosity, with $\delta = 0$ and $\delta = \pi/2$ being equivalent to perfectly elastic and perfectly viscous materials, respectively.

Generally, a storage modulus E' specifies the energy stored in the specimen due to the applied strain, and a loss modulus E'' specifies the dissipation of energy as heat. A useful quantity is the *damping factor* or *loss tangent*

$$\tan\delta = \frac{E''}{E'}, \tag{8}$$

representing a part of mechanical energy dissipated as heat during the loading/unloading cycle. Apparently, it vanishes for a perfectly elastic material and is equal to infinity for a perfectly viscous one. This parameter is linked to the so called *quality factor*, or *Q factor*:

$$Q = \frac{1}{\tan\delta}. \tag{9}$$

The above discussion deals with fundamentals of DMA. In dynamic mechanical analysis tests a harmonic excitation is used with a simultaneous measurement of the amplitudes of stresses and strains as well as the phase angle δ between them. This excitation is low-amplitude so that no plastic deformation could affect the results. Various loading schemes can be used – tensional, torsional and shear. Most materials demonstrate dependence of E', E'' and $\tan\delta$ on frequency and temperature. So, modern DMA testing machines usually perform a test with automatically changing frequencies and temperatures. The latter is important, for instance, for estimation of additional properties such as the glass transitions in polymers.

The scheme overcomes limitations of transferability of results based on the creep and relaxation approach to short-term and high-frequency ranges that are characteristic for various service conditions (Christensen, 1971). As an example, Figure 3 presents results of DMA testing of constituent layers of an adidas football (for details see (Price et al., 2008)). This type of data obtained with DMA can be used to model the visco-elastic behaviour of materials for arbitrary loading conditions and histories. The finite-element software package ABAQUS, for instance, transfers the data for storage and loss moduli into the Prony series (Abaqus, 2003). The latter in the frequency domain will have the following form

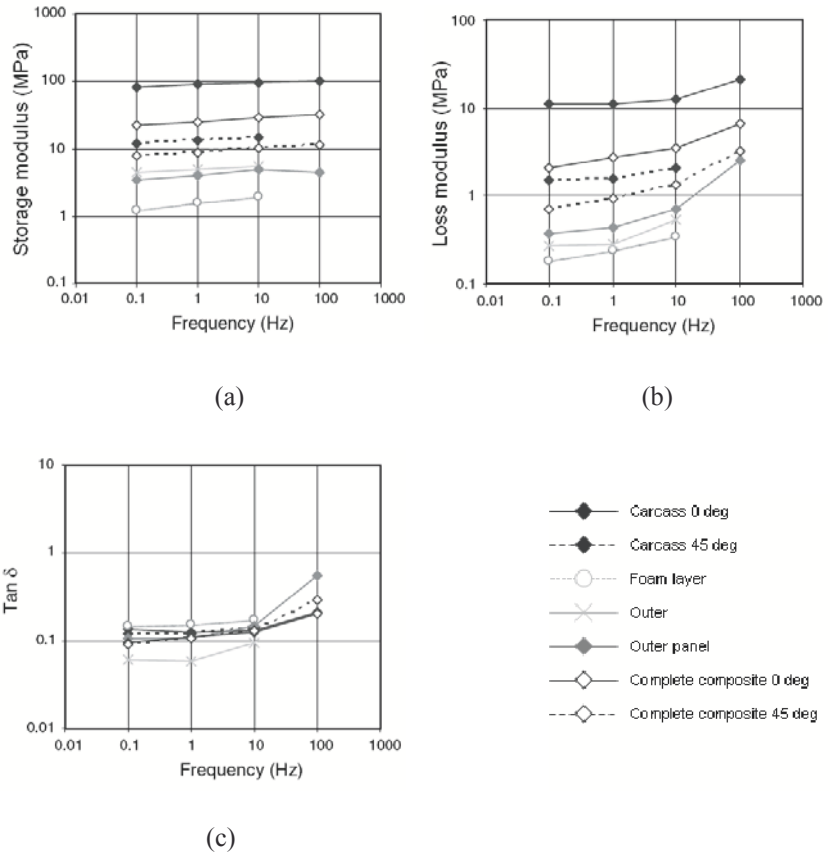

Figure 3. Visco-elastic properties of constituent layers of adidas ball: (a) Storage modulus, (b) loss modulus and (c) $\tan\delta$.

(Park and Schapery, 1999):

$$E'(\omega) = E_e + \sum_{i=1}^{N} \frac{\omega^2 t_{ri}^2}{1+\omega^2 t_{ri}^2} E_i \tag{10}$$

and

$$E''(\omega) = \sum_{i=1}^{N} \frac{\omega t_{ti}}{1 + \omega^2 t_{ti}^2} E_i \,. \tag{11}$$

3 Testing of microspecimens

A scale-dependent mechanical behaviour of materials is well known. With dimensions of tested specimens approaching those of the characteristic elements of microstructure, an averaging effect, which 'smears' both the presence of microstructural features as well as realisation of various deformational mechanisms at lower length scales over a large (macroscopic) volume, diminishes. This can result in significant deviations of the local properties from the global (i.e. averaged) ones. A detailed study of the local properties is important in many cases linked to localisation of deformation and/or fracture processes. Another obvious reason for such studies is linked to applications of components/structures with microscopic dimensions, e.g. in microelectronic packages. In this case, direct testing of microspecimens is unavoidable.

A typical study of lead-free solders at micro scale is analysed here based on works by Gong et al. (2006a, 2007a) and Gong (2007). A process of miniaturisation of microelectronic devices leads to a continuous decrease in the dimensions of all microelectronic components. An additional need to increase the number of interconnections between elements of packages has been driven a diminishment of solder bumps to dimensions below 100 μm. Elements with such dimensions can contain only few grains, making the use of the data obtained for bulk macroscopic polycrystalline specimens at best questionable. To overcome this hindrance, a program of testing at a micro scale was undertaken. A material of interest – lead-free SnAgCu solder – was used in specially prepared specimens. The latter consisted of two Cu plates (15 mm × 15 mm, thickness 1 mm) soldered together by a thin layer of the studied material (Figure 4). A special device was used to change the thickness of the solder layer; in the tests two thicknesses – 100 μm and 1000 μm – were used. The reflow process that transformed the solder paste into solders was implemented with a Planer T-TRACK© reflow oven; two different cooling rates were used to study their effect on the microstructure and properties of solder joints.

After the reflow the specimen was cut with a low-speed diamond saw into specimens with the cross-section 1 mm × 1 mm (see Figure 4b) that were used in mechanical tests. Such specimens can be directly tested in tension using Instron MicroTester. In microelectronic packages solder bumps are exposed to temperature changes resulting in shear deformations due to the mismatch in coefficients of thermal expansion of constituent materials. So, a special setup

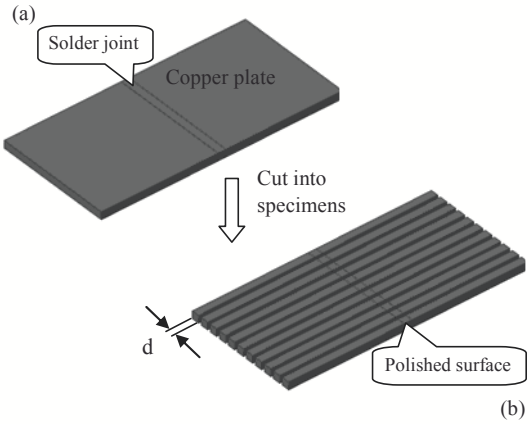

Figure 4. Preparation of microspecimens: (a) specimen after soldering; (b) specimens for the mechanical test. d ≈ 1 mm.

was prepared for testing the manufactured specimens (Figure 5).

A steel holder with a hole, the cross section of which is slightly larger than that of the specimen, is used. It is fixed on one of the testing machine's grips. One of Cu substrates of the specimen is inserted into the hole as shown in Figure 5 while the other substrate at the opposite end is fixed to the machine's second grip, the movement of which is controlled by the MicroTester. Then the hole in the steel holder is filled with Epoxy resin, making sure that the resin does not contact with the solder joint. After 24 hours of curing, the epoxy resin is fully hardened, and the specimen is assembled in the MicroTester in a stress-free state.

In the shear test, the solder joint yields with the copper substrates being still in the elastic state since its yield point is much lower than that of pure copper. At the same time, the Young's modulus of Cu is significantly higher and effectively all the deformation is localised in the solder material. Therefore, the applied engineering shear strain rate $\dot{\gamma}$ on the joint is approximately:

$$\dot{\gamma} = \frac{\dot{U}}{b}. \tag{12}$$

where $\dot{U}$ is the applied displacement rate of the grip and b is the distance

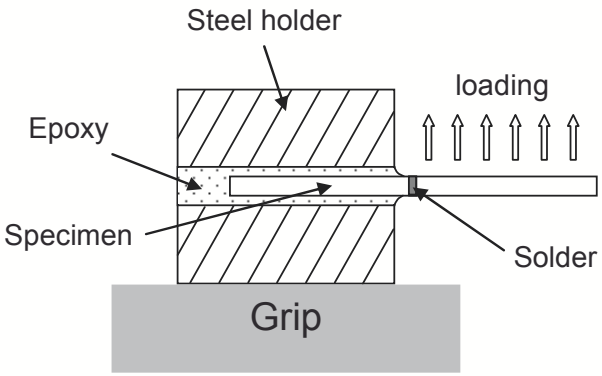

Figure 5. Setup for shear test.

between substrates (it is the distance between the middle points of interfaces for the real specimens). A resin with the highest available stiffness was used in order to reduce its effect on the results.

The mechanical test was performed with the loading rate 0.1 μm/s that corresponds to the shearing strain rate is 1×10^{-3} s^{-1} for solder thickness 100 μm. The specimen at first is loaded for a specific time to reach a prescribed shearing deformation then held in the tester for 24 hours to release the residual stresses.

The microstructure of solder was studied before and after the deformation; both scanning electron microscopy (SEM) and an optical microscopy in polarized light (PL) were employed to examine grain features. Additionally, transmission electron microscopy (TEM) was used to study crystallographic parameters of local areas after loading and to characterize the deformation and damage behaviour of substructures within SnAgCu grains.

A typical result of shear deformation in the solder specimen is presented in Figure 6. Apparently, only two grains occupy the entire cross section of the solder. Their mechanical behaviour is determined by their crystallographic orientation: slip bands inside each grain have the same direction; however, there is a large angle between these bands for the two grains. Shear of stiff, parallel Cu plates induces practically the (macroscopically) uniform deformation state in the solder (with some deviations near the specimen's edges and grain boundaries) of these two grains. Hence, different orientations of shear bands demonstrate the lattice-dependent behaviour and, consequently, anisotropic properties of a SnAgCu single grain. Since a joint in electronic packages can contain one or a

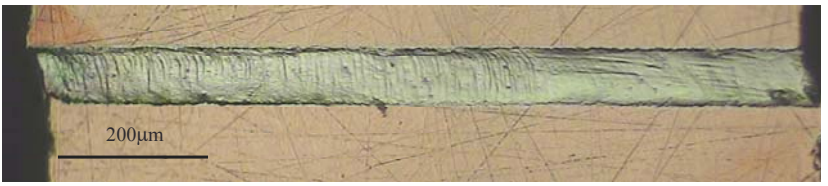

Figure 6. Bright-field image of a loaded joint (b = 82 μm) after shear $\gamma = 39\%$.

few grains, this grain-based behaviour would define its response to the in-service conditions.

The obtained results were used in two-scale finite element analysis of thermal cycling of lead-free joints (Gong et al., 2006b, 2007b and 2008); these results are presented in another Chapter.

In many cases there is a need to analyse even smaller specimens. For instance, the above solder in the test described above still contains more than one grain. To study the intra-grain deformation another technique was used (for details of the method below see (Gong, 2007)). It employed the *focussed ion beam* (FIB) to cur a specimen from the single grain of the solder as shown in Figure 7a. FIB was used to mill the specimen with length and thickness of 25 μm and 2 μm on the ground and polished solder block obtained by the reflow process with a relatively low cooling rate. The bottom of the micro-specimen was separated from the bloc in order to reduce the effect of the bulk specimen and induce a pure tensile deformation state.

This design allows overcoming another limitation of the previous technique – a (relatively) high loading rate. The latter is defined by the minimum displacement rate of the testing machine (that is 0.1 μm/s) and the size of the solder specimen. Since the entire grips' displacement was applied to the solder, in case of the solder layer thickness 100 μm the lowest possible strain rate was 10^{-3} s^{-1}; for the length of the studied micro-specimen it would be even higher – 4×10^{-3} s^{-1}. The use of the bulk solder specimens incorporating the milled micro-specimen can significantly overcome this limit by increasing the length of the bulk specimen (it was 25 mm in the study). With a (nearly) uniform axial distribution of strain in the tensile test the extension rate of the micro-specimen is the same as of the entire specimen. Hence, the strain rate in this test is decreased by a factor equal to the ratio of the length of the macro-specimen to that of the micro-specimen (up to 500 in this study).

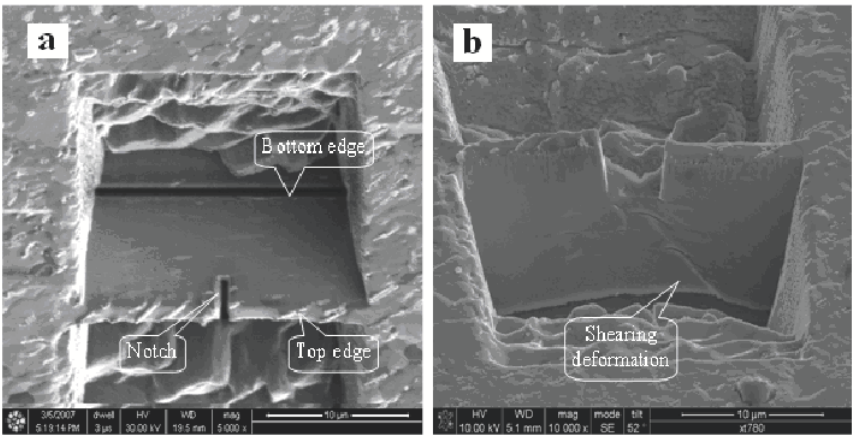

Figure 7. Micro-specimen before (a) and after (b) deformation.

The notch is also introduced into the micro-specimen to study the failure process (Figure 7a). The applied deformation resulted in the strain rate 1×10^{-5} s^{-1}; the specimen after 20% elongation is shown in Figure 7b. The deformed specimen vividly demonstrates the ductile character of deformation – there is no crack growth from the tip of the notch; instead, the notch widens and shear deformation started from the notch at approx. 45° to the tension direction. A further analysis with TEM (gong, 2007) demonstrated that the highly non-uniform character of the deformation process in the single-grain micro-specimen caused by the presence of notch did not only affect the deformation localisation in the form of shear bands but also caused microstructural changes – formation of a low-angle sub-grain boundary.

The two studied cases by no means exhaust possible ways to analyse deformational and failure behaviours at the microscopic scale. Still, they clearly show the considerable increase in the detailedness of information about these behaviours. Besides, a direct effect of microstructure on the spatial realisation of deformational processes and an opposite effect – of the deformation on the microstructure – demonstrate the need for a direct introduction of these processes into respective micromechanical models.

4 Nanoindentation

4.1 Introduction

An apparent difference between the global (macroscopic) and local (microscopic) properties of many advanced materials due to the effects of their microstructure presupposes a development of special techniques for studies at the micro scale. One of the obvious challenges for extension of the conventional testing techniques utilised in universal testing machines to a micro scale is impossibility to perform *in situ* tests in the area of interest. The chance to prepare a micro specimen of the material from this area – though currently feasible with FIB (see above) – still does not fully solve the discussed problem 'specimen *vs*. material' not to mention the complexity of treating such specimens.

Hence, a relatively old idea of the use of indention to measure hardness as a parameter linked to the ratio of the applied force to the effective cross-sectional area of the imprint left by an indentor have become a basis of a new testing technique known as *nanoindentation*. Here, the scaling down is implemented by means of transition to low loads – down to micro-Newtons – resulting in penetration lengths down to nanometres (this is the reason for the name).

Two important moments should be considered here, before a discussion of nanoindentation with its advantages, features and limitations. The first is the use of the free surface of a specimen to measure hardness, and the second is that hardness is *not* a mechanical parameter that can be directly used in any models of mechanics of materials. The former moment presupposes a special attention to preparation of specimens; the latter is alleviated by the use of theories linking hardness to the Young's modulus.

Now, about benefits:

1) Nanoindentation provides a possibility for *en situ* measurements for very small volumes of materials and spatial scale and, hence, can be considered as a *non-destructive* technique.
2) There are options of spatial *scanning* of properties using arrays of indentations points of various configuration and even *continuous* measurements based on nanoscratching (Kaupp and Naimi-Jamal, 2004).
3) A precise placement of the indenting point allows estimation of properties exactly in the area of interest, e.g. in a specific phase, constituent or near any microstructural feature.
4) Automatization of tests allows performing a large testing program, e.g. indentation of the same specimen in many points, without interventions by an operator.

These generic benefits of the method are complementary to the principal feature of nanoindentation, i.e. assessment of properties of materials that

otherwise are hardly feasible. Best examples are soft materials (including biological tissues) and thin (and soft) coatings.

Some limitations of the technique will be discussed after the overview of its main principles, which is based on well-known literature (Fischer-Cripps, 2004, Oliver and Pharr, 1992, 2004, and Pharr and Bolshakov, 2002).

4.2 Principles of nanoindentation

Though the history of hardness tests is several centuries long, their use to extract traditional mechanical properties of materials is significantly shorter. This was linked to a transition from the measurement of the residual area of the imprint to a continuous depth-sensing technique in 1960s (see some historical comments in (Borodich and Keer, 2004); it was known under the name *microindentation* at that time).

The depth-sensing method is based on the continuous measurement of the depth of penetration of indentor h and the corresponding level of the applied force P (see Figure 8). In the process of penetration by indentor into a material the maximum attained level of force applied to the indentor $P_{\max}$ corresponds to the maximum penetration depth $h_{\max}$. Figure 8 also presents other main parameters of the indent's geometry for an axisymmetric (conical) indentor with a half-angle ϕ: the depth of contact h_c and the corresponding radius of the contact circle a; the final depth h_f; the residual imprint depth after unloading (removing of the indentor); the sink-in dept h_s.

Various types of indentors are used for nanoindentation; one of broadly used ones is the Berkovich indentor – a triangular pyramid, made of diamond. It has

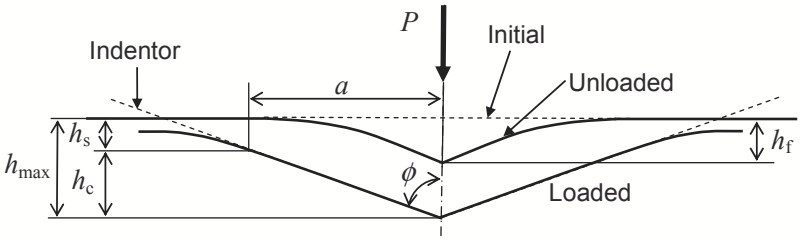

Figure 8. Schematic of indentation process with parameters of indent's geometry (after Oliver and Pharr, 1992).

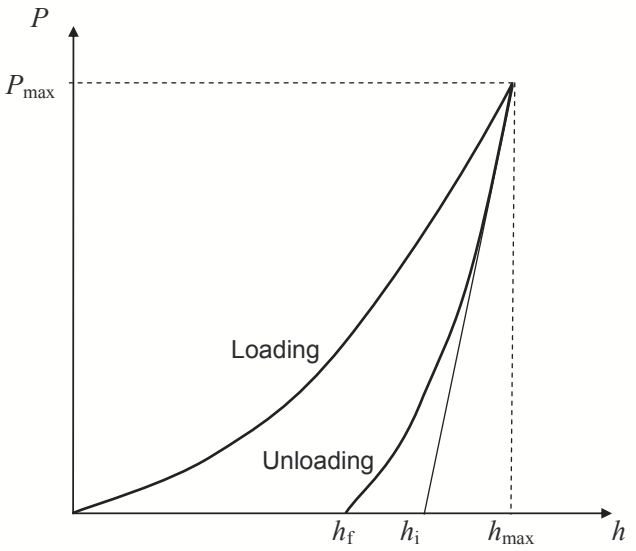

Figure 9. Schematic loading-unloading curve for indentation.

the same area-to-depth relationship as the Vickers indentor, a four-sided pyramid that was used in microindentation tests (Pharr and Bolshakov, 2002). Axisymmetric indentors, including spherical ones, are also used to test various materials.

The continuous measurement of the indentation parameters during the entire cycle of imprinting and removal of the indentor results in the load-displacement (i.e. load-depth) diagram that is schematically presented in Figure 9 (a real curve for a cortical bone tissue is given in Figure 10 (Alam, 2008)). The non-linear loading part of the diagram is followed by an unloading part, situated below the former due to the residual strains caused by the irreversible (plastic in the case of elasto-plastic material) deformation.

The relationships linking the Young's modulus of the tested material and a slope of the initial portion $S = dP/dh$ of the unloading curve were suggested in 1970s (see, e.g. (Bulychev at al., 1975, 1976)). In a more common notation (Oliver and Pharr, 1992, 2004) it can be presented in following form:

$$E_{\text{eff}} = \frac{1}{2\beta}\sqrt{\frac{\pi}{A}}S \tag{13}$$

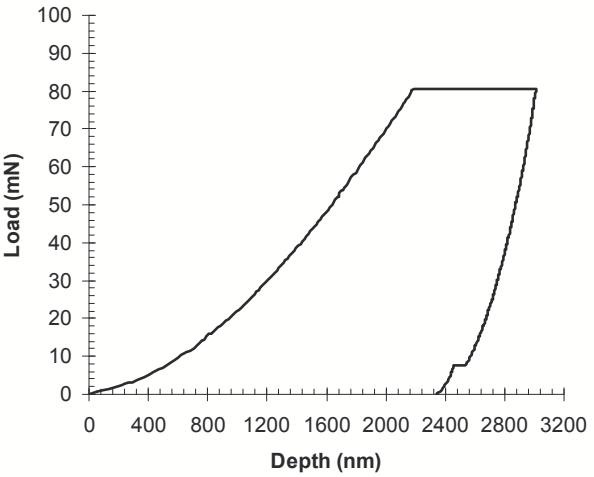

Figure 10. Loading-unloading curve for nanoindentation of cortical bone tissue.

and

$$E_{\text{eff}}^{-1} = \left(1-\nu^2\right)E^{-1} + \left(1-\nu_{\text{i}}^2\right)E_{\text{i}}^{-1}. \tag{14}$$

The system of equations (13), (14) can be resolved with regard to the Young's modulus of the tested material E for a known properties of the indentor – its Young's modulus E_{i} and Poisson's ratio ν_{i} – and the given magnitude of the material's Poisson's ratio ν. Other parameters of the system are the cross-sectional area of the indentor A and the dimensionless parameter β. Theoretically, in approximation of infinitesimal strains, $\beta = 1$ for a rigid axisymmetric indentor penetrating an elastic body. The exact magnitude of β is still a highly discussed area; it is known to depend on the shape of indentor, Poisson's ratio, plastic deformation etc. – a discussion on the matter is given in (Oliver and Pharr, 2004) where the magnitude $\beta = 1.05$ was suggested 'as good a choice as any".

The notion of contact area A is very important to assessing the *hardness* (term *nanohardness* is used for nanoindentation results) of the tested material:

$$H = \frac{P_{\max}}{A}. \tag{15}$$

It is important to note that A is *not* an area of the residual imprint; it is

linked to the contact area *under load*. In effect, it corresponds to the projection of the area of contact when indentor reaches depth $h_{\max}$, i.e. for a case when the depth, along which there is a contact with the indentor, is equal to h_c (see Figure 8).

The current research into applications of nanoindentation is aimed at assessment of additional mechanical properties or parameters. The level of residual stress σ_R can be assessed using the following equation for a spherical indentor with radius R (Fischer-Cripps, 2004):

$$\sigma_R = \sigma_Y - \left[\frac{4E_{\text{eff}}}{3.3\pi}\right]\frac{a}{R}. \tag{16}$$

Nanoindentation can also be used to characterise fracture toughness of materials (Kese and Rowcliffe, 2003), based on the scheme developed for microindentation in 1980s (Lawn et al., 1980). For the known Young's modulus and hardness, the fracture toughness of the tested material can be expressed in the following way:

$$K_c = \alpha\sqrt{\frac{E}{H}}\frac{P}{c_0^{3/2}}, \tag{17}$$

where c_0 is the length of the radial crack, caused by indentation with load P. Parameter α is linked to geometry of indentor (for a cube corner $\alpha = 0.04$ (Field and Swan, 1995)).

The underlying formulae vividly demonstrate limitations of the used approach: this scheme is applicable to isotropic materials with time-independent behaviour. Many novel schemes of applications link results of nanoindentation with detailed finite-element simulations that allow researchers – in many cases by means of inverse analysis – to deal with more complex cases, such as anisotropic materials (Bocciarelli et al., 2005). There are also modifications aimed at alleviation of these limitations – an account for creep is introduced in (Lucas and Oliver, 1999).

4.3 Examples of implementation of nanoindentation

There are various ways to use nanoindentation but – regarding limitations of the method – the most suitable way is to use it for a comparative analysis. The latter can be applied to quantify either the difference in properties of various specimens or the scatter in the spatial distribution of the properties of a single

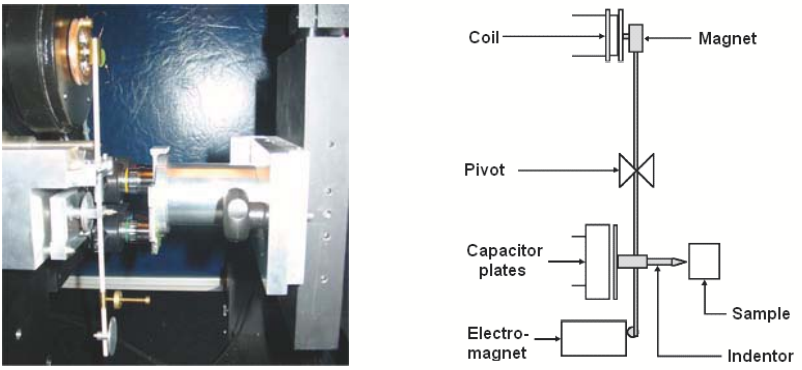

Figure 11. NanoTest Platform: (a) general view; (b) schematic.

material due to its microstructure. This Section presents examples of both approaches.

Effect of Ultrasonically-Assisted Machining. Ultrasonically-Assisted Machining (UAM) is a new technology based on superposition of ultrasonic vibration with amplitude 15-30 μm and frequency around 20 kHz on the movement of the cutting tool (Babitsky et al., 2004). This vibration significantly improves conventional cutting technologies resulting in reduction of cutting forces, improved surface finish etc., allowing turning of hard-to-turn materials such as nickel-based superalloy INCONEL 718. To study the difference between the conventional turning (CT) and ultrasonically-assisted turning (UAT), it is necessary to understand the extent of the effect of technology on the sub-surface layers of machined specimens. Hence, nanoindentation tests were performed with the NanoTest Platform made by Micro Materials Ltd, Wrexham, UK (Figure 11) to estimate the layer affected by turning.

The specification of the range and sensitivity for the displacement and load is shown in Table 1.The Berkovich indenter is used in all the tests.

In NanoTest Platform a load to the indentor is applied by means of a coil and magnet located at the top end of the pendulum. The penetration of the probe into the sample is monitored with a sensitive capacitive transducer. In order to prepare a specimen for the nanoindentation analysis, parts of work pieces that were machined with CT and UAT were placed facing each other and potted into

Table 1. Specification of the NanoTest Platform.

Displacement range and sensitivity	
Range	0-50 μm
Noise-floor	0.025% of full-scale deflection
Theoretical resolution	0.04 nm
Load range and sensitivity	
Maximum resolution	better than 100 nN
Load ranges	up to 0-500 mN
X/Y/Z resolution/travel	0.02 mm/50 mm
Analysis area	50 mm × 50 mm

epoxy resin as it is shown in Figure 12a. After polishing the produced specimen was mounted into the NanoTest machine (Mitrofanov, 2004, and Ahmed et al., 2006). The tests were carried out in an automatic mode with a total duration of two days. There are three runs A, B and C, parallel to each other (vertical lines in Figure 12b). Each of these lines goes from the conventionally machined part of the specimen, crosses a thin separating layer of plastic between samples and then goes through the workpiece sample machined with UAT. Each run consisted of three parts: coarsely placed indents (with the distance of 50 μm between two neighbouring indentation points) in the regions distant from the machined surfaces and finely placed indents (with spacing 10 μm) in the direct vicinity of the machined surfaces.

Each indentation point was produced with a constant load of about 10 mN applied to the probe tip. The difference in the residual depth of the indent produced with the probe is automatically recalculated into hardness and the Young's modulus of the corresponding indentation place as it is shown above.

Results of nanoindentation for INCONEL 718 machined with two turning techniques (Figure 13) vividly demonstrate that at distances from the machined surfaces larger than 100 μm the measured levels of nanohardness converge to a relatively low level that should correspond to that for the non-machined (as-delivered) state of the alloy. Sub-surface layers are significantly harder for both techniques, and both the level of hardness and depth of the affected layer are higher for CT.